JOURNAL OF AIRCRAFT
Vol. 45, No. 2, March–April 2008

Engineering Notes

ENGINEERING NOTES are short manuscripts describing new developments or important results of a preliminary nature. These Notes should not exceed 2500 words (where a figure or table counts as 200 words). Following informal review by the Editors, they may be published within a few months of the date of receipt. Style requirements are the same as for regular contributions (see inside back cover).

Transient Structure on Unmanned Combat Air Vehicle: Effect of Pitch-Up Motion

M. Elkhoury*
Lebanese American University, Byblos, Lebanon

DOI: 10.2514/1.32609

I. Introduction

FLIGHT envelopes of unmanned combat air vehicles (UCAV) planforms demand high performance at high angle of attack when undergoing dynamic motions. Up to this point, studies of the present UCAV planform have focused primarily on the flow structure on stationary planforms at defined angles of attack (static conditions), with varying Reynolds number. The dynamic effects of a perturbed or pitching motion on the flow structure of the planform have received less attention.

Nearly all investigations have addressed the flow structure on a delta wing under dynamic conditions, whereby the wing has a relatively large sweep angle, in comparison with the low values of sweep of a UCAV planform. Among these, LeMay et al. [1] studied the dynamics of vortices on a pitching delta wing, and Miller and Gile [2] examined the effect of blowing on delta wing vortices during pitching. A basic finding is that the location of vortex breakdown, compared with the static case, is further upstream during pitch-up motion and further downstream during pitch-down motion. This phase lag becomes larger with increasing pitch rate.

Myose et al. [3] studied the effects of more complex planforms, including diamond, cropped, delta, and double-delta configurations. Emphasis was on vortex breakdown during pitching. Their main finding was that the cropped delta wing, which resembles the fuselage-apex form of the present UCAV, had the latest onset of leading-edge vortex breakdown during pitching, whereas the double-delta wing had the earliest onset. This observation may be one of the reasons underlying new designs of complex UCAV planforms.

For a double-delta wing undergoing pitching motion, Ericsson [4] described the consequences of large-amplitude pitching oscillations at high angle of attack, whereas Grismer and Nelson [5] studied the aerodynamics of pitching motion with and without sideslip. Grismer et al. [6] and Hebbar et al. [7] also examined the influence of sideslip on the control of vortical flow structure on such planforms.

Modern military aircraft involve complex, novel shapes such as the present UCAV (approximating the Boeing X-45) to incorporate stealth technology. For such planforms, Elkhoury and Rockwell [8] provided dye visualization images over a range of angle of attack and Reynolds number, accounting for the potential interaction of the coexistence of vortices emanating from the apex and the wing root, and the onset of vortex breakdown. Elkhoury et al. [9] employed a particle image velocimetry (PIV) technique to investigate the crossflow plane and near-surface topology by determining the mean and unsteady representations of their flow structure at various ranges of angle of attack and Reynolds number. However, none of the investigations so far have addressed the influence of unsteady maneuvers, such as the effect of a sudden increase of the angle of attack on the flow structure. Hence, the aim of the present investigation is to provide insight into the transient flow structure at a specific location normal to the planform surface, which takes place on a generic aerodynamic planform undergoing pitch-up motion at various ramp rates.

Received 4 June 2007; revision received 25 July 2007; accepted for publication 27 July 2007.

*Assistant Professor, Department of Mechanical Engineering, Post Office Box 36; mkhoury@lau.edu.lb.

II. Experimental System and Techniques

Experiments were performed in a large-scale water channel, with a test section 927 mm wide, 610 mm deep, and 4928 mm long. The freestream velocity was set to $U_\infty = 53.4$ mm/s corresponding to a Reynolds number of $Re = 10,000$ based on the chord of the planform, which was $C = 188$ mm. The wing had a thickness of 3.2 mm, and was beveled on its windward side at an angle of 30 deg. The apex of the fuselage and the wing root had sweep angles of 45 and 40 deg, respectively. The angle of attack was varied in a ramplike motion over a range of 2–15 deg. The UCAV planform was held in position using a streamlined strut that was 2.5 mm thick extending normal to the surface. A stepping motor mounted above the free surface was used for the pitch-up motion. The pitching axis was located approximately at the midchord of the planform.

A PIV technique with a dual-pulsed Yag laser system, having a maximum output of 90 mJ was employed for imaging in the crossflow plane. Schematics that represent the planform showing the crossflow imaging orientation are given in Fig. 1. All images were taken at a streamwise distance corresponding to $x/C = 0.644$, in which x is the distance measured from the nose of the planform. The flow was seeded with 12 μm, metallic-coated hollow plastic spheres, which were essentially neutrally buoyant. The collinear beam from the laser head was passed through a system of cylindrical and spherical lenses. Images were deflected exterior to the test section via a small mirror as shown in the schematic. Because of symmetry and to optimize the special resolution of the flowfield, images were acquired over half of the planform. Laser reflection from the surface of the planform during imaging in the crossflow plane precluded accurate determination of the patterns of velocity in the region close to the planform surface.

Images were recorded by a high-resolution charge-coupled device (CCD) camera, whose axis was perpendicular to the vertical wall of the test section. This high-resolution CCD camera had an array of 1024×1024 pixels, of which 1008×1016 were light sensitive with an effective framing rate of 15 cps. The size of the interrogation window was 32×32 pixels corresponding to a grid size of $\Delta/C = 0.00762$. The effective overlap was 50%, to satisfy the Nyquist criterion.

III. Effect of Transient Motion on Flow Structure on an X-45 UCAV Planform

The planform was subjected to a linear-ramp motion, and its effect on the relaxation process of the flow structure was studied. The

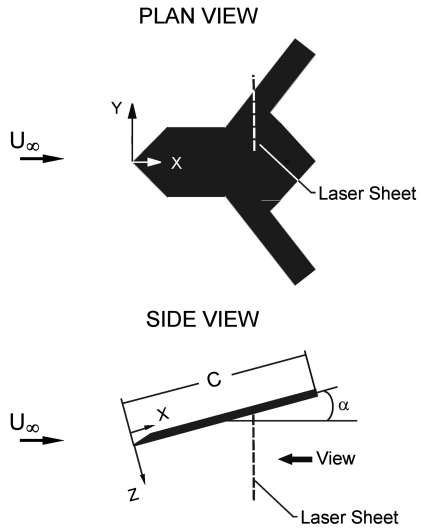

Fig. 1 Overview of UCAV planform and laser sheet locations, and orientations for crossflow imaging.

planform was pitched from 2–7 deg over a time interval Δt of 0.33 s, corresponding to a dimensionless ramp rate of $\dot{\alpha}C/2U \approx 0.93$ and from 2–15 deg over two different time intervals Δt of 0.86 and 11 s, corresponding to dimensionless ramp rates of $\dot{\alpha}C/2U \approx 0.93$ and $\dot{\alpha}C/2U \approx 0.073$, respectively. All these dimensionless ramp rates fall within the flight envelope of most UCAVs. Acquisition of data started as soon as the planform reached its final angle of attack. Hence, increasing values of N designated on each image corresponds to increasing values of time after the cessation of motion. At $N = 5$, the value of the dimensionless time $tU/C = 0.095$. At successive values of $N = 15, 20, 40$, and 160, the corresponding values of tU/C are 0.284, 0.378, 0.757, 3.029, respectively.

A. Patterns of Instantaneous Vorticity, Streamline, and Surface-Normal Velocity Component for High Pitch Rate

For the pitch rate $\dot{\alpha}C/2U \approx 0.93$, with initial and final angles of attack $\alpha_i = 2$ deg and $\alpha_f = 7$ deg, a sequence of crossflow states is indicated in Fig. 2. At $N = 5$, the instigation of the vortex core is clearly evident and designated as a, which results in a high vorticity level ω labeled as b. The corresponding image of surface-normal velocity is shown to the right of the figure. The highest negative peak level of velocity at e is generally maintained throughout the whole sequence of images. It is a result of the high velocity emanating from the windward side of the planform. The other positive and negative are peaks designated as f and g, respectively. The core of the vortex lies at the zero level between the maximum gradients located at h_1. At $N = 15$, a positive bifurcation line, i.e., convergence of streamlines toward a common line, is clearly identifiable in the surface-normal streamline. Two new peaks of vorticity labeled as c and d are evident and the location g disappears from the instantaneous surface-normal velocity patterns. The relaxation process starts around $N = 20$ where the surface-normal streamline pattern shows a degradation in the vortex core, with no major changes in both the vorticity and the surface-normal velocity contours. There is a very slight difference between the patterns at $N = 40$ and those at $N = 160$. Hence, one may conclude that the relaxation process is qualitatively almost complete around $N = 40$ for this ramp case. It is worth noting that only a single core is evident in all streamline topology for $N > 160$

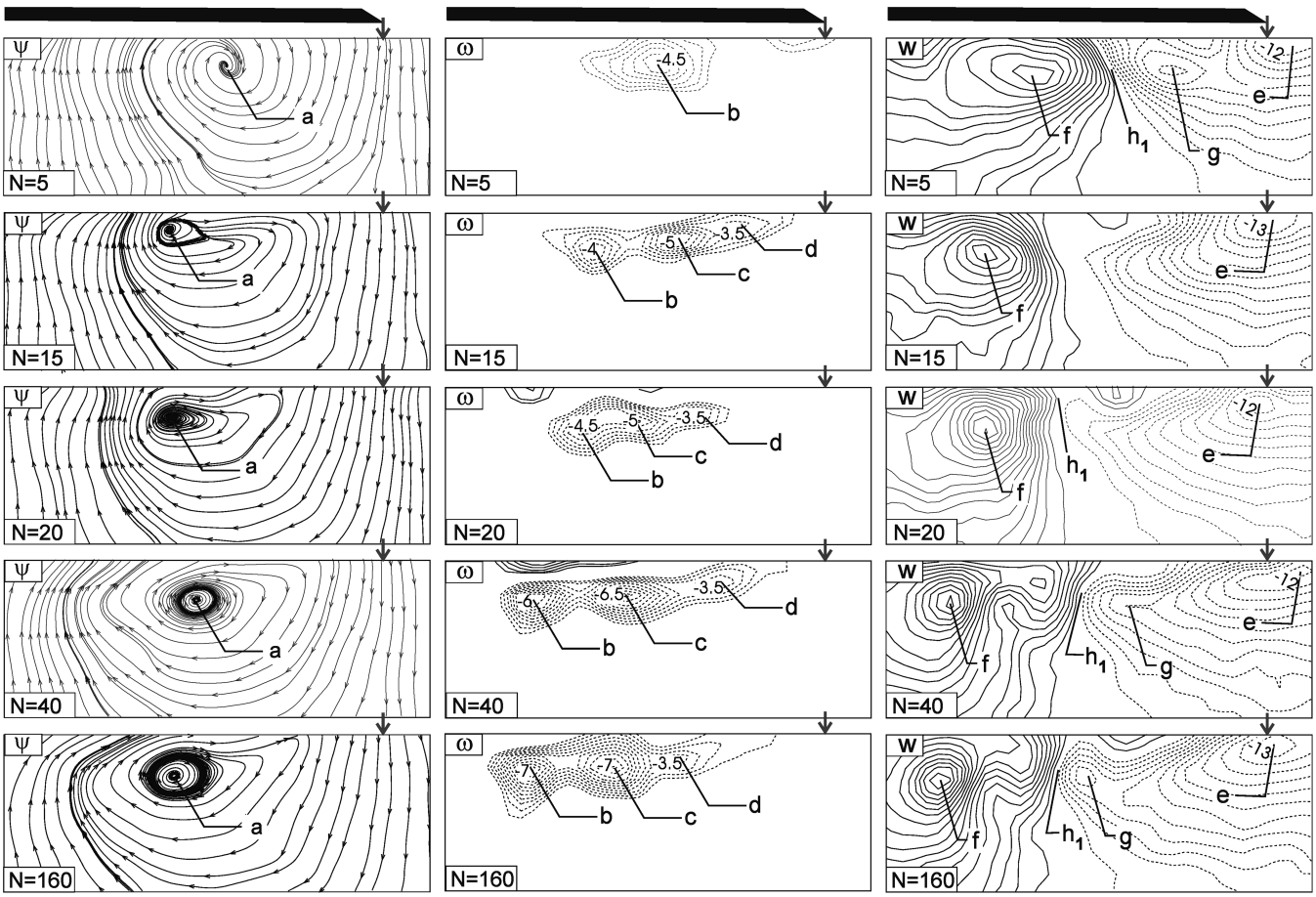

Fig. 2 Transient patterns of instantaneous streamline topology ψ, vorticity ω, and velocity contours W in the crossflow plane as a function of frame number N after completion of a linear-ramp pitching motion between initial and final angles of attack $\alpha_i = 2$ deg and $\alpha_f = 7$ deg over a time interval $\Delta t = 0.33$ s corresponding to $\dot{\alpha}C/2U = 0.93$. Minimum level of W and minima of ω are shown on each image with units of mm/s and $\sec^{-1}$, respectively. The incremental value of W and ω are 1.0 mm/s and 0.5 $\sec^{-1}$, respectively.

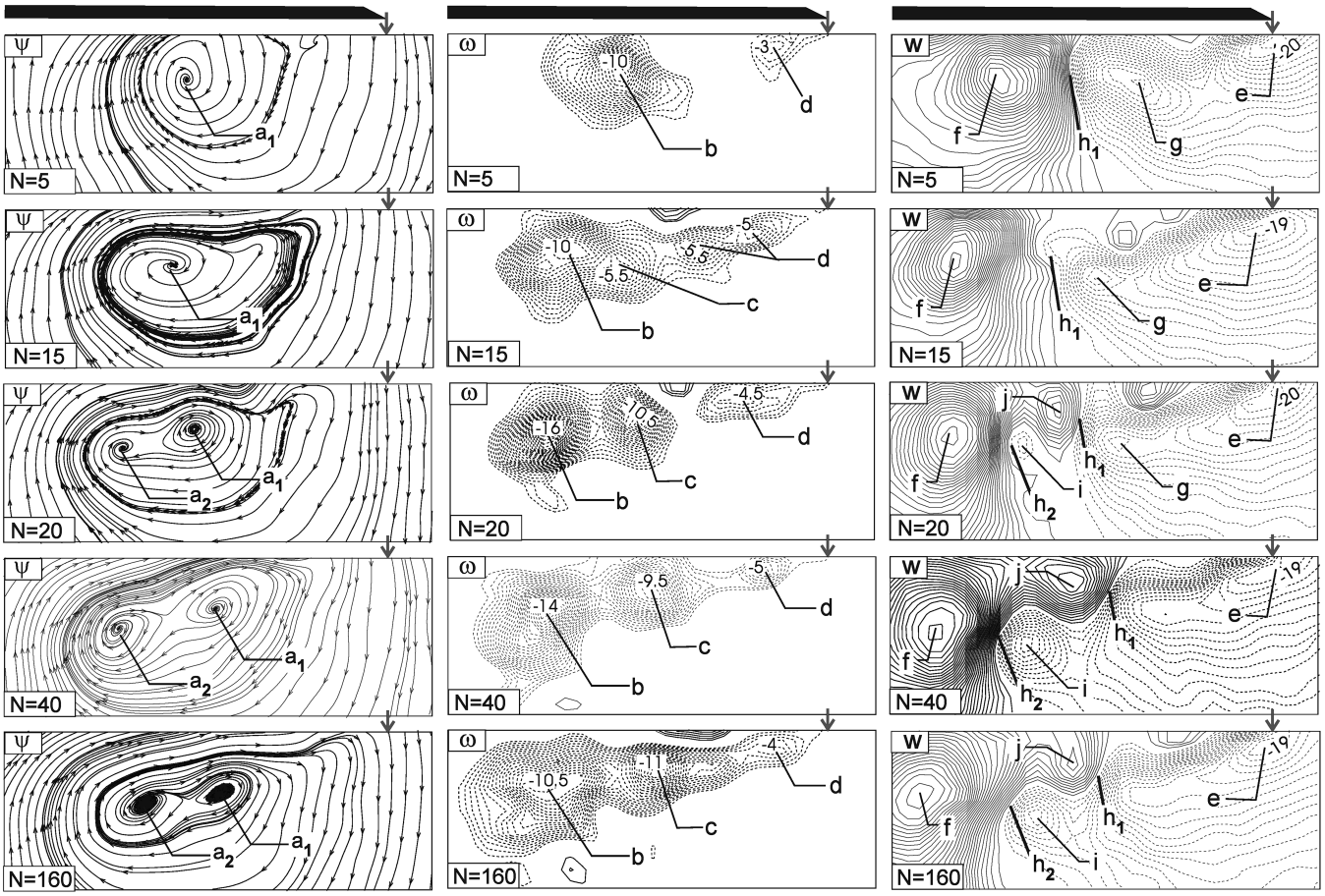

Fig. 3 Transient patterns of instantaneous streamline topology ψ, vorticity ω and velocity contours W in the crossflow plane as a function of frame number N after completion of a linear-ramp pitching motion between initial and final angles of attack $\alpha_i = 2$ deg and $\alpha_f = 15$ deg over a time interval $\Delta t = 0.86$ s corresponding to $\dot{\alpha}C/2U = 0.93$. Minimum level of W and minima of ω are shown on each image with units of mm/s and $\sec^{-1}$, respectively. The incremental value of W and ω are 1.0 mm/s and 0.5 $\sec^{-1}$, respectively.

due to intertwining of vortices emanating from the apex and wing root.

Next, we consider the case that corresponds to a pitch-up from an initial angle of attack of $\alpha_i = 2$ deg to a final angle of attack of $\alpha_f = 15$ deg, at the same nondimensional pitching rate. The corresponding streamline patterns, vorticity, and surface-normal velocity contours are shown in Fig. 3. At $N = 5$, the streamline patterns and the surface-normal velocity contours are qualitatively very similar to the previous case. However, the peak in the vorticity contours labeled as d is clearly identifiable at this stage. A single core a_1 that corresponds to the apex vortex is present in the streamline patterns and similar peaks occur in the patterns of surface-normal velocity, as for the aforementioned case. At $N = 15$, the vortex core a_1 slightly moves inward; this corresponds to movement of the peak g in the surface-normal velocity contours in the same direction. A new vorticity peak, designated as c, develops and all peaks slightly move inward.

At $N = 20$, there are no major changes in the vorticity contours. However, a second vortex core, corresponding to the wing root vortex designated as a_2, is evident in the streamline patterns. Two new peaks in the surface-normal velocity contours, designated as i and j, are clearly identifiable as a result of a newly formed vortex, represented by h_2, which corresponds to zero level of the surface-normal velocity component that lies at the center of the vortex core. At $N = 40$, a new vortex core a_2 is more obvious and is associated with a prominent peak i in the surface-normal velocity contours. At $N = 160$, the flow structure is very similar to that at $N = 40$, which therefore indicates that the relaxation process has come to completion around $N = 40$.

B. Cross Comparison of High and Low Pitching Rates

At the same nondimensional pitching rates, the relaxation process was nearly complete at $N = 40$ for the previous two cases, despite the difference in flow structures at different angles of attacks. To determine how the relaxation process depends on the pitch rates and to investigate the development of flow structures during transition at different pitch rates, the following comparison is considered. The low pitching rate corresponding to $\dot{\alpha}C/2U = 0.073$ is given in Fig. 4. At $N = 5$, there is only the apex vortex core a_1 in the streamline patterns. The three vorticity peaks, namely b, c, and d are clearly evident in the vorticity contours. The surface-normal velocity contours at $N = 5$ are similar to those of the high pitching rate case at $N = 15$.

At $N = 15$, in Fig. 4, the formation of the wing root vortex core designated as a_2 is evident in the streamline topology and the three peaks in the vorticity contours are clearly defined. Furthermore, the peak labeled as j is evident, indicating the initial formation of the second vortex and the peak labeled as i just forms in the contours of surface-normal velocity. Note that this peak is clearly seen at $N = 20$ for the case of the high pitching rate. The vortex core a_2 seems to be more developed (and has a higher peak level designated as i) at the low pitching rate, when compared with the case of the high pitching rate at $N = 20$. However, it seems that the formation of the second vortex core a_2 was slowly evolving for the low pitching rate when compared with that of the high pitching rate case. Comparison of streamline topology and surface-normal velocity contours at $N = 40$ and 160, indicates similar structure for both cases, which in turn suggests that the relaxation process is qualitatively near completion at $N = 40$.

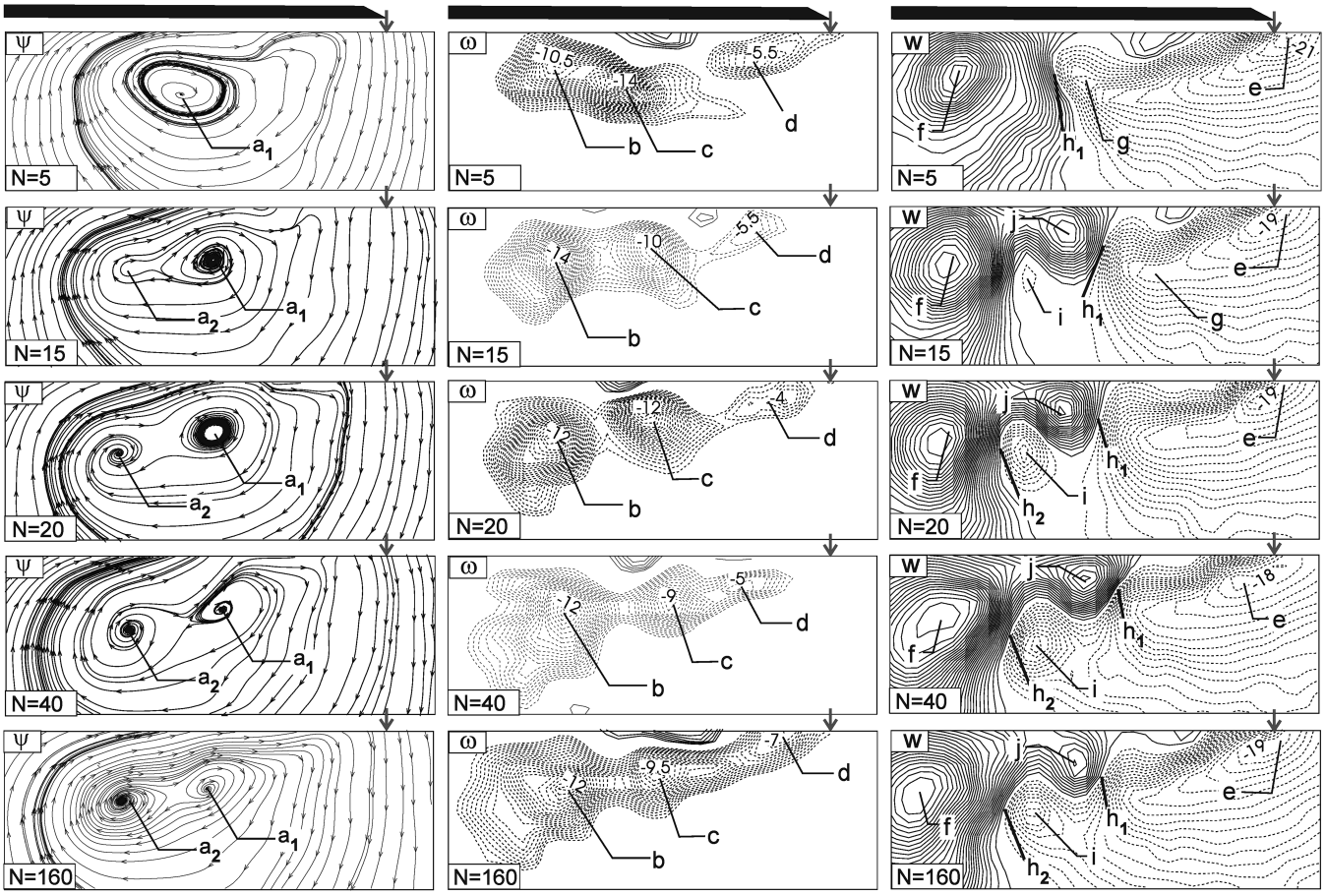

Fig. 4 Transient patterns of instantaneous streamline topology ψ, vorticity ω and velocity contours W in the crossflow plane as a function of frame number N after completion of a linear-ramp pitching motion between initial and final angles of attack $\alpha_i = 2$ deg and $\alpha_f = 15$ deg over a time interval $\Delta t = 11.0$ s corresponding to $\dot{\alpha}C/2U = 0.073$. Minimum level of W and minima of ω are shown on each image with units of mm/s and $\sec^{-1}$, respectively. The incremental value of W and ω are 1.0 mm/s and 0.5 $\sec^{-1}$, respectively.

IV. Conclusions

The relaxation process of flow structure in the crossflow plane on an X-45 planform has been investigated as a function of the pitch-up rate. Comparisons of patterns of streamline topology, surface-normal velocity, and vorticity provides quantitative representation of the dependency of the relaxation process on the pitch-up rate. The principal findings are as follows:

1) Low pitch rates yield quicker development of flow structure, as represented by the onset of manifestation of the wing root vortex core. However, it seems that the vortical structure associated with low pitch rates slowly evolves when compared with high pitch rates for the same dimensionless time.

2) For the same nondimensional pitch rate, in spite of the difference of the final angle of attack for the two cases considered herein, the flow structure has very similar patterns at the beginning of the relaxation process.

3) The final form of the flow structure becomes evident at approximately $tU/C = 0.378$ ($N = 20$) for all cases, regardless of the pitching rate. Furthermore, the flow structure appears to be fully evolved at approximately $tU/C = 0.757$ ($N = 40$) for all three cases considered herein.

Acknowledgments

The author is grateful to Donald Rockwell for allowing him to use the laboratory facilities at Lehigh University and to M. Metin Yavuz for his assistance in conducting the preceding experiments.

References

[1] LeMay, S. P., Batill, S. M., and Nelson, R. C., "Vortex Dynamics on a Pitching Delta Wing," *Journal of Aircraft*, Vol. 27, No. 2, 1990, pp. 131–138.

[2] Miller, L. S., and Gile, B. E., "Effects of Blowing on Delta Wing Vortices During Dynamic Pitching," *Journal of Aircraft*, Vol. 30, No. 3, 1993, pp. 334–339.

[3] Myose, R. Y., Lee, B. K., Hayashibara, S., and Miller, L. S., "Diamond, Cropped, Delta, and Double-Delta Wing Vortex Breakdown During Dynamic Pitching," *Journal of Aircraft*, Vol. 35, No. 3, 1997, pp. 567–569.

[4] Ericsson, L. E., "Vortex Characteristics of Pitching Double-Delta Wings," *Journal of Aircraft*, Vol. 36, No. 2, 1999, pp. 349–356.

[5] Grismer, S. D., and Nelson, C. R., "Aerodynamic Effect of Sideslip on Double-Delta Wings," AIAA Paper 93-0053, Jan. 1993.

[6] Grismer, S. D., Nelson, C. R., and Ely, W. L., "Influence of Sideslip on Double Delta Wing Aerodynamics," *Journal of Aircraft*, Vol. 32, No. 2, 1995, pp. 451–453.

[7] Hebbar, S. K., Platzer, M. F., and Chang, W. H., "Control of High-Incidence Vortical Flow on Double-Delta Wings Undergoing Sideslip," *Journal of Aircraft*, Vol. 34, No. 4, July–Aug. 1997, pp. 506–512.

[8] Elkhoury, M., and Rockwell, D., "Visualized Vortices on Unmanned Combat Air Vehicles Planform: Effect of Reynolds Number," *Journal of Aircraft*, Vol. 41, No. 5, 2004, pp. 1244–1246.

[9] Elkhoury, M., Yavuz, M. M., and Rockwell, D., "Near-Surface Topology of an Unmanned Combat Air Vehicles Planform: Reynolds Number Dependence," *Journal of Aircraft*, Vol. 42, No. 5, Sept.–Oct. 2005, pp. 1318–1330.